Characterization of Disulfide Bonds in Human Nucleoside Triphosphate Diphosphohydrolase 3 (NTPDase3): Implications for NTPDase Structural Modeling†

Vasily V. Ivanenkov,[#] Jarek Meller,[‡] and Terence L. Kirley*,[#]

Department of Pharmacology and Cell Biophysics, College of Medicine, University of Cincinnati, P.O. Box 670575, Cincinnati, Ohio 45267-0575, and Biomedical Informatics, Children's Hospital Research Foundation, Cincinnati, Ohio

Received November 30, 2004; Revised Manuscript Received April 6, 2005

ABSTRACT: Cell-surface nucleotidases (NTPDases) contain 10 invariant cysteine residues in their extracellular regions. To investigate disulfide structure in human NTPDase3, we made single and double mutants of these 10 cysteines, and analyzed their enzymatic activity, glycosylation pattern, trafficking to the cell membrane, and sensitivity to reduction. The mutants constituted five distinct phenotypes, thus, strongly suggesting disulfide bonds between C92−C116 (first bond), C261−C308 (second bond), C289−C334 (third bond), C347−C353 (fourth bond), and C399−C422 (fifth bond). Due to conservation of the 10 cysteines, the identified five disulfide bonds are likely to exist in all cell-surface NTPDases. The third and fifth bonds are also present in the soluble NTPDases and are critical for processing, trafficking, and enzymatic activity. The fourth bond has minimal effect on processing and function, while the first and second bonds are of intermediate importance. Most of the N-linked glycosylation sites in the wild-type enzyme are processed to complex oligosaccharides, but at least one site is high-mannose or hybrid in structure. Interestingly, disruption of the first disulfide bond resulted in some enzyme that lost sensitivity to endoglycosidase H, suggesting that the first disulfide bond in the wild-type enzyme shields some high-mannose glycans from terminal glycosylation. Comparative modeling by threading and homology modeling of the NTPDase3 sequence revealed a high degree of structural fold similarity with a bacterial exopolyphosphatase (PDB 1T6C). The resultant theoretical 3-D model of the extracellular portion of NTPDase3, based on homology with this exopolyphosphatase, is consistent with the assignment of the disulfide bonds occurring in regions of good fold similarity between NTPDase3 and the exopolyphosphatase. The 3-D model obtained for NTPDase3 also suggests the structural basis for the importance of several apyrase conserved regions for the nucleotidase activities of the NTPDases.

The NTPDases are a family of eight known enzymes, which hydrolyze nucleotides outside the cell (NTPDase1−3 and 8),[1] in the lumen of intracellular membranes such as the ER and Golgi (NTPDase4 and 7), or in both locations (NTPDase5 and 6) (*1*). NTPDase1−4, 7, and 8 share the same membrane topology, having two membrane-spanning domains located near the N- and C-termini. NTPDase5 and 6 are found both in intracellular membrane organelles as integral membrane proteins and, after cleavage of an N-terminal signal peptide, are released into the extracellular media as soluble enzymes. The differential nucleotide hydrolysis properties and relative efficiency of hydrolysis of various nucleoside di- versus triphosphates are important for distinguishing the functions of the various NTPDase family members. The NTPDases found on the cell surface, including the NTPDase3 that is the subject of this study, are thought to modulate signaling mediated by cell-surface purinergic receptors. These purinergic receptors control many physiological processes, including blood clotting, pain perception, and smooth muscle contraction (*2*).

We are interested in the determination of structural elements principal for nucleotidase activity and specificity of NTPDase enzymes, because this information can be used to validate protein structural models and to help design modified enzymes of the proper hydrolytic specificity to be useful as therapeutic proteins. For this reason, we have recently expressed in bacteria the soluble forms of NTPDase6 (*3*) and NTPDase5 (*4*) and, after refolding, obtained enzymes with high specific nucleotidase activities. Other authors (*5*) have crystallized and done extensive site-directed mutagenesis to make an unrelated nucleotidase, the human soluble calcium-activated nucleotidase (hSCAN (*6*−*8*)), much better at hydrolyzing ADP, and therefore developed a potential

† This work was supported by NIH grants HL59915 and HL72882 to T. L. K.

* Address correspondence to Dr. Terence L. Kirley, Department of Pharmacology and Cell Biophysics, University of Cincinnati College of Medicine, 231 Albert Sabin Way, Cincinnati, OH 45267. Phone: 513-558-2353. Fax: 513-558-1169. E-mail: terry.kirley@uc.edu.

[#] University of Cincinnati.

[‡] Children's Hospital Research Foundation.

[1] Abbreviations: DTT, dithiothreitol; Endo H, endoglycosidase H; ER, endoplasmic reticulum; NEM, *N*-ethylmaleimide; NTPDase3, nucleotide triphosphate diphosphohydrolase 3; PBS, phosphate-buffered saline; PNGase, peptide *N*-glycosidase F; PPX/GPPA, exopolyphosphatase/guanosine pentaphosphate phosphohydrolase.

10.1021/bi047487z CCC: $30.25
Published on Web 06/04/2005

therapeutic anticoagulant protein. However, while soluble NTPDases may be amenable for crystallization and 3-D determination, they are not necessarily good models for the membrane-bound members of the same family (NTPDases1−4 and 7−8) since the soluble forms are monomeric, and contain only two disulfides, whereas the cell-surface NTPDases (NTPDases1−3 and 8) are all oligomeric and all contain 10 conserved cysteine residues, presumably forming five conserved disulfide bonds.

Molecular modeling is an increasingly useful and important approach for characterizing the 3-D structure of the cell-surface NTPDases, since, like most integral membrane proteins, they are not currently amenable for crystallization. Knowledge of disulfide architecture is of principal importance for building the models. Disulfide bonds contribute spatial constraints since they define the regions of the primary structure that must be in proximity to each other in the 3-D structure. Consequently, the knowledge of disulfide bond arrangement is critical for both construction and evaluation of the 3-D models. Therefore, we are interested in identification of disulfide bonds in NTPDases. Using chemical techniques, we have recently determined the two disulfide bonds in bacterially expressed, soluble NTPDase6 (*3*). However, cell-surface expressed NTPDases have a more complex disulfide structure, since they contain 10 conserved cysteines in their extracellular regions that are presumably paired in five disulfides. To elucidate the arrangement of disulfide bonds in the membrane-bound NTPDase3, we used a mutagenesis approach, since the more direct protein chemical approach is not feasible due to the limiting amounts of protein generated by the COS cell expression system, as well as to the higher complexity of the disulfide structure. This mutagenesis approach has been used in many systems to identify or confirm the location of disulfide bonds (*9*−*14*), including the disulfide assignment for P_2X receptors (*15*, *16*), which share the same membrane topology (N- and C-terminal membrane-spanning regions flanking a large extracellular loop) with the membrane-bound NTPDases. Unique phenotypes caused by mutation of each of the 10 conserved cysteines, singly and in pairs, strongly suggest the presence of five disulfide bonds, which are likely to exist in all the cell-surface NTPDases since all of them contain the corresponding invariant 10 cysteines in their extracellular regions. The disulfide structure obtained helped us to evaluate the accuracy of a computational 3-D model of the extracellular region of NTPDase3, which is based on comparative modeling using the recently described crystal structure of the exopolyphosphatase/guanosine pentaphosphate phosphohydrolase (PPX/GPPA) enzyme (*17*) as a template.

MATERIALS AND METHODS

Site-Directed Mutagenesis of NTPDase3. Mutagenesis of the wild-type NTPDase3 in pcDNA3 vector was performed by using the QuikChange II site-directed mutagenesis kit (Stratagene) as described (*18*). The DNA Core Facility at the University of Cincinnati produced the synthetic oligonucleotides and sequenced all the cDNA constructs to verify the presence of correct mutations.

Transient Transfection and Preparation of COS Cell Membranes. COS-1 cells were transfected with 4 μg plasmid DNA per 100 mm plate using Lipofectamine and Plus reagents (Invitrogen). Transfection with an empty pcDNA3 vector was also performed as a control. Approximately 48 h post-transfection, the COS-1 cells were harvested, and the crude cell membrane preparations were obtained as described (*19*).

Protein Assay. Protein concentrations were determined using the Bio-Rad protein assay reagent with the modifications of Stoscheck (*20*), using bovine serum albumin as the standard.

Nucleotidase Assays. Nucleotidase activities were determined by measuring the amount of inorganic phosphate (P_i) released from nucleotide substrates in the presence of 5 mM Ca^{2+}, at 37 °C, using a modification of the technique of Fiske and Subbarow (*21*) as described (*18*). The enzyme assay was initiated by the addition of ATP or ADP to 2.5 mM final concentration.

SDS−PAGE and Western Blotting. Pre-cast 10-well or 15-well 4−15% gradient minigels (Bio-Rad) were used for SDS−PAGE. In most experiments, proteins were run in the gels for approximately twice the time needed for the Bromphenol Blue dye to reach the bottom of the gels, to improve the resolution in the molecular weight range of the NTPDase3 protein. After electrophoresis, the proteins were electrotransferred to Immun-Blot PVDF membrane (Bio-Rad) and processed as described (*22*), using a 1:5000 dilution of polyclonal antisera and incubation overnight at 21 °C, and a 1:2000 dilution of secondary Stabilized Goat Anti-Rabbit HRP-Conjugated antibody (10 μg/mL stock concentration, obtained from Pierce) for 1 h at 21 °C. Immunoreactivity was detected by chemiluminescence using SuperSignal West Dura Extended Duration Substrate (Pierce) and was recorded using FluorChem IS-8800 system (Alpha Innotech) or Blue Autorad Film (BioExpress). Two rabbit anti-NTPDase3 polyclonal antibodies, designated KLH1 and KLH11, were used. KLH1 antibody was generated against the C-terminal peptide (amino acid residues 515−529) of NTPDase3 (HB6) protein and has been previously described (*22*). KLH11 antibody was generated against the internal amino acid sequence (^{311}DQRPESYNPNDVITFEG^{327}), which was predicted by computation using the Gene Runner program (Emini surface probability (*23*)) to be exposed on the protein surface and to be antigenic (Figure 1). This antibody produced a stronger and more specific signal with NTPDase3 compared to KLH1, and therefore, the KLH11 antibody was used unless otherwise indicated.

Deglycosylation. Deglycosylation was performed using PNGase or Endo H (New England Biolabs) according to the manufacturer's instructions. NTPDase3 in crude membrane preparations was solubilized with 0.2% Triton X-100 containing 1 mM EDTA and 2% of Protease Inhibitor Cocktail Set III (Calbiochem) for 30 min at 21 °C, and then centrifuged in a Beckman air-driven centrifuge (Airfuge) for 20 min at 100 000*g*. The supernatant was combined with 10× Glycoprotein Denaturing Buffer (0.5% SDS and 1% β-mercaptoethanol final concentrations) and boiled for 10 min. Each sample was then divided into aliquots, combined with the appropriate reaction buffers (New England Biolabs), and incubated with either PNGase or Endo H at 37 °C for 1 h or for 3 h. Similarity of deglycosylation patterns in these aliquots indicated the completeness of the deglycosylation reaction after 1 h. The controls were incubated under the same conditions but without glycosidases. After incubation,

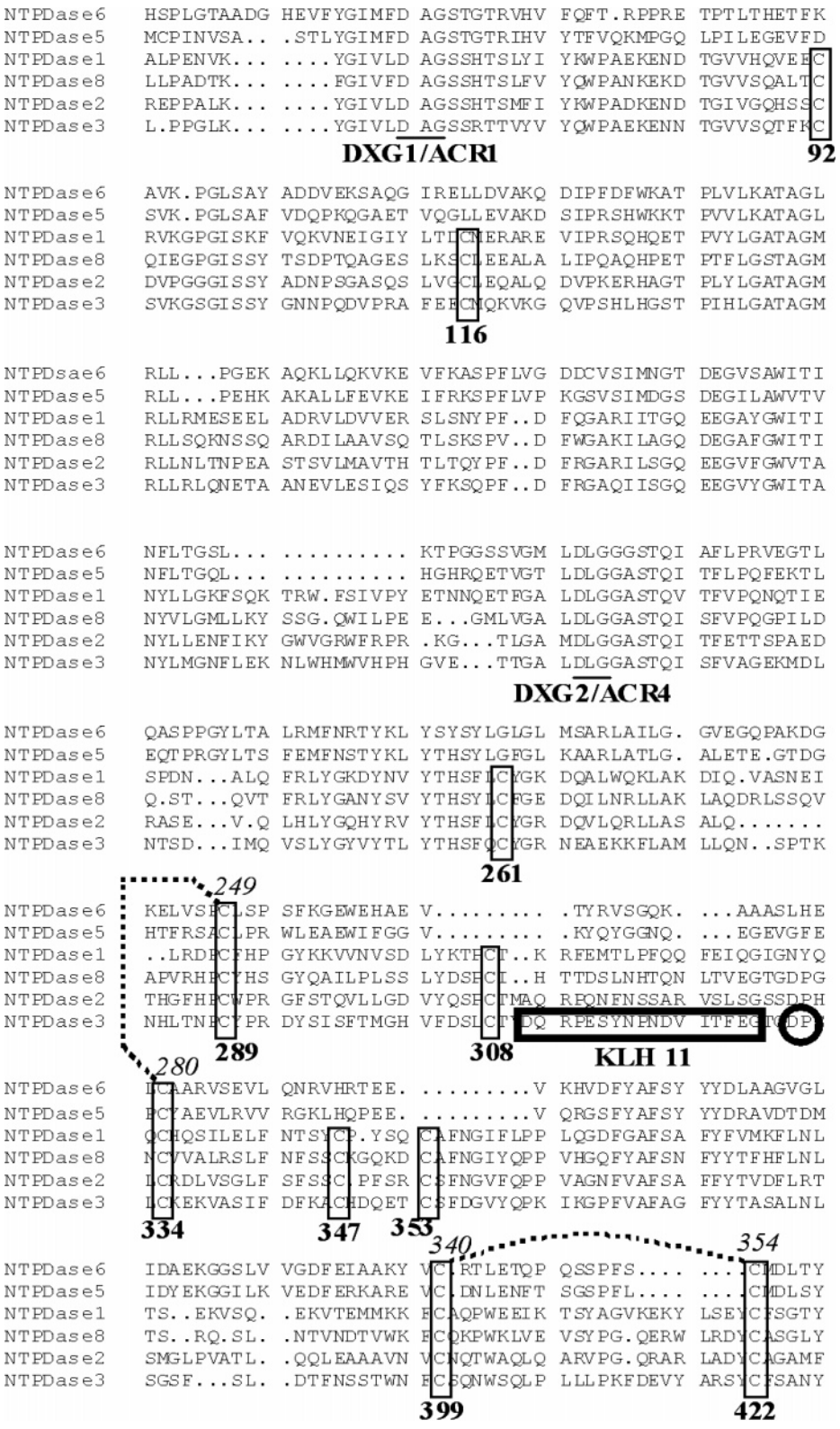

FIGURE 1: Ten cysteine residues are invariant in the extracellular region of cell-surface NTPDases(1−3 and 8). The four cell-surface NTPDases(1−3 and 8) are aligned with two soluble NTPDases(5 and 6) using the PRETTY multiple sequence alignment program, which is part of the SeqWeb suite of analysis programs based on the Genetics Computer Group (GCG) Wisconsin computer analysis programs. The portion of the alignment containing the 10 extracellular conserved cysteines is shown, and these cysteines are marked by vertical boxes, with the numbers beneath the boxes corresponding to the NTPDase3 sequence. Two disulfide bonds in NTPDase6, which have been identified by chemical techniques (*3*), are shown by two dotted lines, and the numbers of the paired cysteines in the soluble form of NTPDase6 are indicated above the boxes in italics. Two DXG motifs within ACR1 and ACR4 are underlined. The boxed KLH11 sequence corresponds to the peptide used to generate the KLH11 antibody utilized extensively in this work. The single Asp−Pro peptide bond uniquely susceptible to acid cleavage under mild conditions is encircled. Accession numbers for the human sequences shown are AF039916 (NTPDase6), AF039918 (NTPDase5), AAB47572 (NTPDase1), AY3644442 (NTPDase8), AAB81013 (NTPDase2), and AF034840 (NTPDase3).

the samples were combined with SDS loading buffer containing 200 mM DTT and analyzed by Western blotting.

Biotinylation of Cell-Surface Proteins. Cell-surface proteins were biotinylated with either EZ-Link Sulfo-NHS-LC-Biotin (Pierce) that reacts with primary amine groups or N^{α}-(3-maleimidylpropionyl)biocytin (biotin maleimide) from Molecular Probes that reacts with sulfhydryl groups. Both reagents are impermeable to the plasma membrane under the conditions used and, therefore, were used to label the extracellular part of NTPDase3. Plates (100 mm) containing transfected COS-1 cells were placed on ice and washed twice with ice-cold PBS. Biotinylation with EZ-Link Sulfo-NHS-LC-Biotin (0.5 mg/mL in PBS, pH 7.5) was performed for 1 h at 4 °C. Cells were then washed with ice-cold PBS and incubated with a quenching buffer (50 mM glycine in PBS) for 10 min at 4 °C. Cells were harvested by scraping in buffer (30 mM MOPS−NaOH, pH 7.4, 2 mM EDTA, 250 mM sucrose, and 50 mM glycine) and processed for cell membrane preparation (*19*). Biotinylation with biotin-maleimide (500 μM in PBS, pH 7.0) was performed for 1 h at 4 °C. After incubation, the cells were washed with ice-cold PBS and incubated with a quenching buffer (5 mM cysteine in PBS) for 10 min at 4 °C. Cells were scraped in buffer (30 mM MOPS−NaOH, pH 7.4, 2 mM EDTA, 250 mM sucrose, and 1 mM cysteine) and processed for cell membrane preparation (*19*). Crude membrane preparations were solubilized with 0.2% Triton X-100 containing 1 mM EDTA and 2% of Protease Inhibitor Cocktail Set III (Calbiochem) for 30 min at 21 °C, and then centrifuged in an Airfuge for 20 min at 100 000*g*. The supernatants were diluted with TBS buffer (150 mM NaCl and 20 mM Tris-HCl, pH 7.3) containing 1% Triton X-100 and incubated with 15 μL ImmunoPure Immobilized Streptavidin agarose beads (Pierce) for 20 h with end-over-end rotation at 4 °C. Beads were then washed three times with TBS containing 1% Triton X-100, and biotinylated proteins were eluted by re-suspending the beads in SDS loading buffer containing 200 mM DTT and boiling for 5 min. Beads were pelleted by centrifugation, and the supernatant was analyzed by Western blotting for detection of biotinylated cell-surface expressed NTPDase3 protein.

Oxidative Sulfhydryl Cross-Linking With Copper Phenanthroline. The stock solution of Cu(II)(1,10-phenanthroline)$_3$ was 150 mM $CuSO_4$ and 500 mM 1,10-phenanthroline in 4:1 water/ethanol as described (*24*). Membrane preparations were diluted with 30 mM MOPS−NaOH, pH 7.4, to a protein concentration of 0.2 mg/mL, and copper phenanthroline was added to a final concentration of 3 mM. The reaction was carried out for 30 min at 21 °C and then quenched by adding 2 vol of nonreducing SDS loading buffer containing 20 mM EDTA and 40 mM NEM.

Acid Hydrolysis at the Unique Asp330−Pro331 Peptide Bond in NTPDase3. Membranes from COS cells transfected with C10S or C10S/C261S/C308S NTPDase3 mutants (2 mg/mL protein concentration) were combined with an equal volume of extraction buffer (30 mM MOPS, pH 7.4, 2% Triton X-100, and 4 mM NEM), incubated 30 min at 21 °C, and then centrifuged for 20 min at 100 000*g*. The supernatants were transferred into screw-capped thermal cycler tubes (Thermolyne); HCL was added to the final concentration of 20 mM (final pH $\approx$ 1.75), and the samples were incubated in an oven for 17 h at 70 °C. Each sample was then analyzed under both reducing and nonreducing conditions by combining half of the sample with SDS loading buffer containing 200 mM DTT (reducing conditions) and another half with SDS loading buffer containing 2 mM NEM (nonreducing conditions), followed by SDS−PAGE and Western blotting.

Computer Analyses and Modeling. We used sequence alignment and fold recognition methods to identify putative homologues and build structural models of NTPDase3 and other related NTPDases. Psi-BLAST (*25*) was used to detect weak sequence homologies with NTPDase3. Several fold recognition servers were used to identify structural homologues by threading the primary sequence of the extracellular portion of NTPDase3 through databases of known 3-D protein structures, including two well-benchmarked (e.g., in subsequent CAFASP evaluations (*26*)) and reliable servers, namely, FUGUE (http://www-cryst.bioc.cam.ac.uk/fugue/ (*27*)) and FFAS (http://bioinformatics.ljcrf.edu/FFAS/ (*28*)). Secondary structure and solvent accessibility predictions were generated using PsiPRED (http://globin.bio.warwick.ac.uk/psipred/ (*29*)), SABLE (http://sable.cchmc.org (*30*)), and PROFsec (http://ubic.bioc.columbia.edu/predictprotein) servers to compare these predictions with the template proteins. We then used homology modeling and the SCWRL server (http://www.fccc.edu/research/labs/dunbrack/scwrl/ (*31*)) to obtain putative 3-D models of the NTPDase3 structure based on the FUGUE and FFAS alignments. Additional fold recognition searches were performed using LOOPP (http://cbsu.tc.cornell.edu/software/loopp/ (*32*)) and 3D-PSSM (http://www.sbg.bio.ic.ac.uk/~3dpssm/ (*33*)) servers to look for homologues of sequence fragments of the NTPDase3 extracellular sequence.

The FFAS- and FUGUE-derived NTPDase3 3-D models were evaluated by the Verify3D program (*34*−*36*), using both the stand-alone version and a Web server version available at http://www.doe-mbi.ucla.edu/Services/Verify_3D/. In particular, the FUGUE model file (FUGUE_NTPDase3_3D_coordinates.pdb), which is included in the Supporting Information for this study, was analyzed by Verify3D. This Verify3D output file was annotated to show the positions of the NTPDase3 ACR regions and cysteine residues and is included in the Supporting Information for this study (filename, Verify3D_NTPDase3_FUGUE_Model.jpg). Using Verify3D, we also performed analyses of the quality of homology-refined models obtained using the SCWRL server and the initial FFAS and FUGUE alignments (data not shown).

RESULTS

Effects of Cysteine Mutations on Enzymatic Activity and Glycosylation. Cell-surface NTPDases (NTPDase1−3 and 8) contain 10 invariant cysteines in the extracellular region (Figure 1). The conservation of these cysteines suggests their involvement in five disulfide bonds, since it has been established that the disulfide-paired cysteines (cystines) are generally conserved, in contrast to nonconserved cysteines with free sulfhydryl groups (*37*). To identify the disulfide structure, we took a mutagenesis approach that is based on the assumption that mutation of either of two cysteines connected in a disulfide bond would result in the same enzymatic phenotype as mutation of both residues. Accordingly, we disrupted the putative disulfide bonds by mutating

Table 1: NTPDase3 Mutations Made for Disruption of Putative Disulfide Bonds

putative disulfide bond(s) disrupted	mutations
	Mutations Disrupting One Putative Disulfide Bond
1	C92S, C116S, C92S/C116S
2	C261S, C308S, C261S/C308S
3	C289S, C334S, C289S/C334S
4	C347S, C353S, C347S/C353S
5	C399S, C422S, C399S/C422S
	Mutations Disrupting Two Putative Disulfide Bonds
1 + 2	C92S/C261S, C116S/C261S, C92S/C308S, C116S/C308S
1 + 5	C92S/C399S, C92S/C422S, C116S/C399S, C116S/C422S
2 + 3	C261S/C289S, C308S/C334S
2 + 5	C308S/C399S, C308S/C422S
	Mutations in C10S Background
2	C10S/C261S/C308S
4	C10S/C347S, C10S/C353S

[a] Mutations in C10S background were used for experiments requiring nonreducing conditions. The C10S mutation removes Cys10 from the N-terminal cytoplasmic tail and results in a fully active, wild-type-like enzyme (*55*). This mutation eliminates the spurious dimerization of the protein via intersubunit disulfides formed by Cys10, which occur to varying degrees during COS cell membrane preparation of wild-type NTPDase3 under nonreducing conditions (*55*).

each of the 10 extracellular cysteines to serine, individually and in pairs (Table 1), and analyzed the mutant phenotypes regarding the residual ATPase activities and glycosylation states (Figure 2). We then arranged the 15 single and double cysteine mutants into phenotypic groups, such that each group contained mutants of similar phenotypes, distinct from the other groups. By this means we established five distinct groups, suggesting the cysteines within each group are disulfide-paired (Figure 2).

The effects of cysteine substitution ranged from a complete inactivation of the enzyme (e.g., C289S, C334S, and C399S) to a slight decrease in ATPase activity (e.g., C347S, C353S, and C347S/C353S), as shown in Figure 2A. Cysteine mutations affected the glycosylation state of the enzyme to various degrees as shown by Western blotting (Figure 2B). All protein bands seen in the blot represent various states of N-glycosylation of the core protein (approximately 55 kDa), since removal of all *N*-glycans by treatment with PNGase converted all electrophoretic bands of all mutants to the size of the core protein band (only PNGase-treated WT enzyme is shown in Figure 2B, lane 17). The C347S, C353S, and C347S/C353S mutants, which exhibit almost wild-type nucleotidase activities, are also very similar to wild-type regarding their glycosylation patterns (Figure 2B, lanes 11−13). In contrast, cysteine mutants C289S, C334S, and C289S/C334S that are devoid of nucleotidase activity are represented by a single band of approximately 66 kDa (Figure 2B, lanes 8−10). The increased mobility of this band compared to that of wild-type suggests an impaired and incomplete glycosylation. Electrophoretic patterns of other cysteine mutants consist of two molecular forms: a band of the same mobility as wild-type and a band of partially glycosylated molecules indicating an altered glycosylation. An interesting feature of the C92S, C116S, and C92S/C116S mutants is the presence of an additional band with electrophoretic mobility lower than that of wild-type (the faint band marked with an asterisk in Figure 2B, lanes 2−4). This band likely represents a hyper-glycosylated protein, a hypothesis supported by the deglycosylation analysis described below.

Thus, these 15 cysteine mutants can be arranged in five distinct groups regarding their ATPase activities and glycosylation patterns, so that in each group phenotypes of single and double mutants are similar (Figure 2A,B). On the basis of the assumption that replacement of either of two cysteine residues forming a disulfide bond would result in the same phenotypes as replacement of both residues, the putative disulfide bonds are assigned as shown in Figure 2B,C. While disulfide bonds 1, 4, and 5 connect cysteine residues in a sequential manner in the primary structure, disulfide bonds 2 and 3 are overlapping.

Phenotypic Effects of Double Cysteine Mutations That Disrupt Two Disulfide Bonds. To verify the assignment of disulfide bonds, we investigated the effects of 12 double cysteine mutations that disrupt two putative disulfide bonds (Table 1). We reasoned that if the assignment of disulfides shown in Figure 2C is correct, then phenotypes of double mutations disrupting two disulfide bonds would be different from, and more detrimental than, phenotypes of single mutations disrupting one disulfide bond. All 12 double mutants exhibited the same electrophoretic pattern, and therefore, only three of them are shown in Figure 3, lanes 3, 6, and 9. Double mutants (e.g., C116S/C308S, lane 3 in Figure 3) differ from single mutants (e.g., C116S and C308S, lanes 1 and 2 in Figure 3) in that double mutants lack both the natively glycosylated protein band and the residual nucleotidase activity. Because the phenotypes of double mutants are different from phenotypes of single mutants, the mutated cysteines are likely to belong to different disulfide bonds. Thus, phenotypic analyses of these double mutants support the assignment of disulfide bonds shown in Figure 2C.

Analysis of Glycosylation State of Cysteine Mutants. Because the assignment of disulfide bonds in this study utilizes the comparison and interpretation of electrophoretic patterns of mutated NTPDase3, we investigated the molecular basis for the electrophoretic forms of the enzyme. As described above, treatment of WT and all mutants with PNGase converted all protein bands into a single band of the core protein of about 55 kDa (data for WT are shown in Figure 2B, lane 17). This indicates that all molecular forms of NTPDase3 seen in Western blots represent various N-glycosylation states of the core protein. NTPDase3 has seven putative N-glycosylation sites in the extracellular region (*19*), and it was shown that glycosylation of NTPDase3 (*22*, *38*) and the related NTPDase1 (*39*, *40*) is essential for enzymatic activity and proper cell-surface localization of the enzymes. We further characterized the types of N-linked oligosaccharides associated with the altered electrophoretic mobility of cysteine mutants by deglycosylation analysis with Endo H. Endo H specifically recognizes and hydrolyzes the high-mannose *N*-glycans (*41*) that are characteristic for immature proteins resident in the ER (*42*). While some high-mannose glycans may escape terminal glycosylation in Golgi and be present in mature glycoproteins (*43*), most *N*-glycans in mature proteins are processed to complex oligosaccharides and are resistant to Endo H digestion (*42*).

To analyze glycosylation states of cysteine mutants, we solubilized the COS membrane proteins with 1% Triton X-100 and prepared 100 000*g* supernatants. This treatment

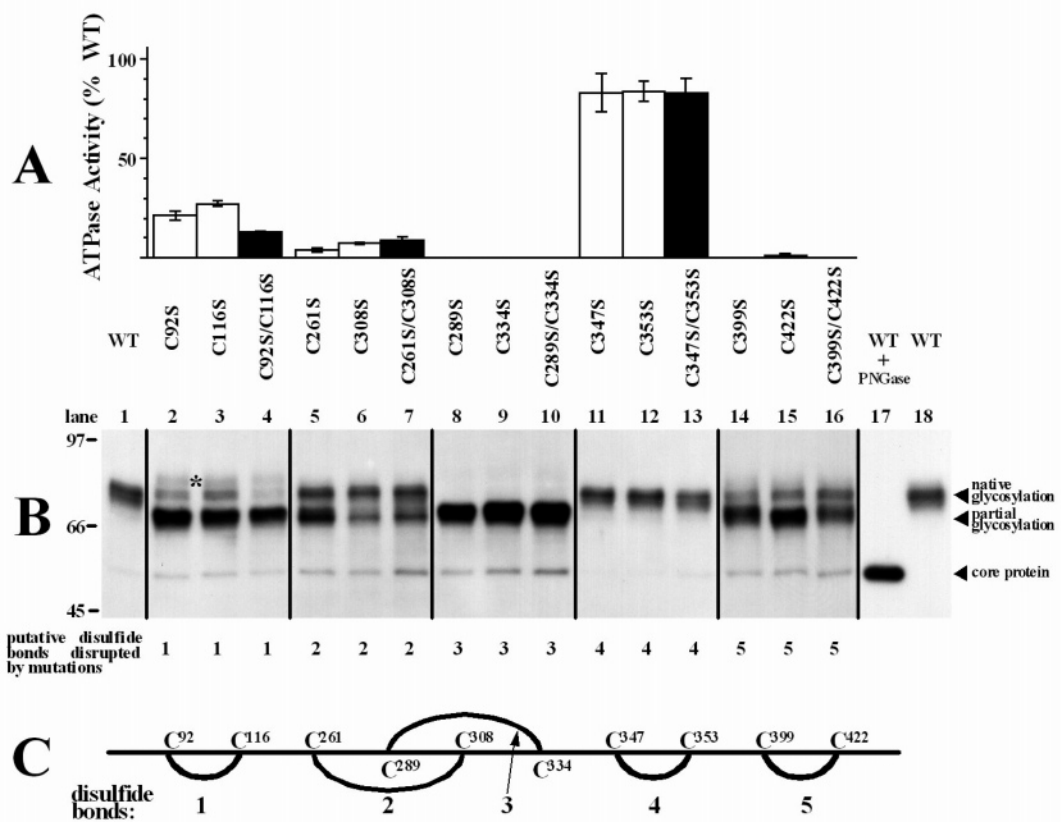

FIGURE 2: Cysteine mutants constitute five groups of phenotypes regarding their nucleotidase activities and glycosylation states. (A) ATPase activity of cysteine mutants. COS cells were transfected with wild-type and mutant NTPDase3 plasmid DNA in triplicate. ATPase activities were assayed using the same amount of COS membrane protein per assay, and the activities are expressed as percentage of the wild-type ATPase activity. Residual activities less than 1% of wild-type were considered to be zero and were not plotted. White and black bars correspond to single and double mutants, respectively. Values represent means ± SD of three transfections. (B) Glycosylation states of cysteine mutants as revealed by Western blotting. Protein bands with electrophoretic mobility similar to that of wild-type are marked as "native glycosylation" since they exhibited similar properties in Endo H analysis, and they represent the enzyme that is delivered to the cell surface (see also Figures 4 and 5). In contrast, the lower protein bands with higher electrophoretic mobility are marked as "partial glycosylation" since they represent high-mannose glycoproteins, which neither completed terminal glycosylation nor were delivered to the cell surface (see also Figures 4 and 5). The asterisk indicates the hyper-glycosylated protein band with decreased electrophoretic mobility compared to that of wild-type, which is characteristic of single and double mutations of C92 and C116. A small amount of nonglycosylated core protein is seen in the WT, and this band is more pronounced in most cysteine mutants. Lane 17 shows the conversion of the wild-type natively glycosylated form to the core protein after treatment with PNGase. (C) Disulfide bond assignments based on results shown in A and B, and in Figure 3. Disulfide bonds are depicted as the arcs connecting the paired cysteines.

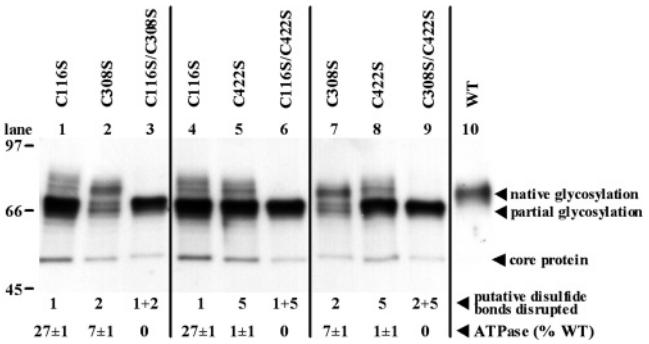

FIGURE 3: Double cysteine mutations involving two disulfide bonds completely inactivate the enzyme and abolish native glycosylation. Glycosylation states were analyzed by Western blotting. Putative disulfide bonds disrupted by cysteine mutations are indicated below the blot. The same protein amounts of transfected COS cell membranes were used to assay ATPase activities given below the blots. Values are given as means ± SD of three transfections. Note that disruption of an additional disulfide bond in the double mutants eliminated the residual ATPase activity and abolished the protein band corresponding to the natively glycosylated enzyme.

solubilized all natively glycosylated and active molecular forms of NTPDase3 but did not effectively solubilize, and therefore greatly diminished, the abundance of the partially glycosylated forms, which would otherwise obscure the minor native bands (compare lanes 5 and 6 in Figure 4A). An additional advantage of using the Triton X-100 extracts is that they do not contain the nonglycosylated core protein, simplifying the interpretation of electrophoretic patterns after Endo H treatment, which reduces the apparent molecular mass of some bands to that of the core protein.

Treatment of wild-type NTPDase3 with Endo H slightly reduced the apparent molecular mass (Figure 4A, lanes 2 and 3) indicating that at least one N-glycosylation site in the mature enzyme is high-mannose or hybrid in structure. However, the shift in electrophoretic mobility caused by Endo H treatment is small compared to the position of the nonglycosylated core protein, indicating that most of the N-glycosylation sites in the mature wild-type enzyme are processed to complex oligosaccharides. Endo H analysis revealed three types of glycoforms in cysteine mutants, which differed in their response to Endo H treatment. All three types are seen as separate bands in the C92S mutant (Figure 4A, lane 6). The molecular mass of the lower band was decreased to that of the nonglycosylated core protein indicating that

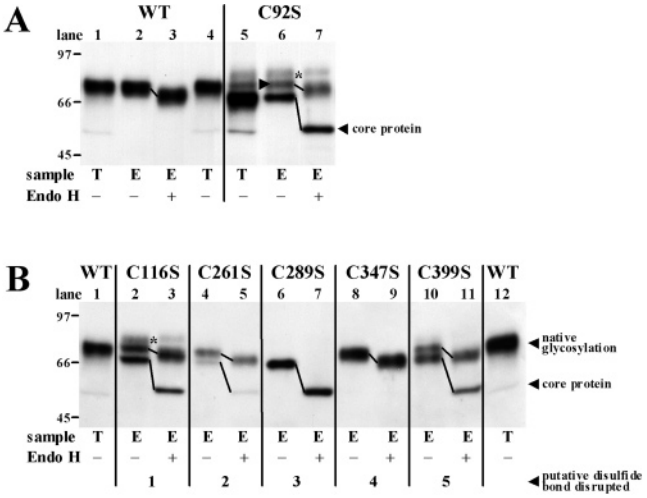

FIGURE 4: Disruption of various disulfide bonds impairs NTPDase3 processing to varying degrees and results in accumulation of immature, high-mannose type, glycoproteins. (A) Wild-type (WT) and C92S mutant were solubilized with Triton X-100 (100 000*g* supernatant) and subjected to treatment with Endo H. E, Triton X-100 soluble extract; T, total sample obtained by dissolving COS membranes directly in SDS loading buffer. A small amount of nonglycosylated core protein can be seen in wild-type total (T) samples, and this band is more abundant in the C92S mutant (T). (B) Cysteine mutants representative of each of five phenotypes shown in Figure 2B were solubilized with Triton X-100 and analyzed for sensitivity to Endo H as in A. Wild-type total (T) samples (lanes 1 and 12) are given for comparison. Putative disulfide bonds disrupted by cysteine mutations are indicated below the blot.

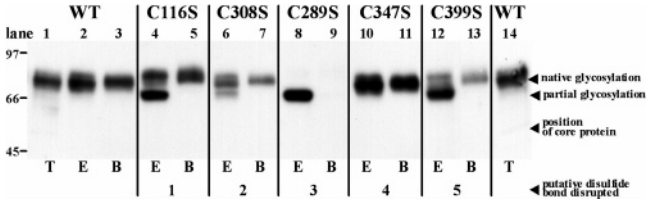

FIGURE 5: Cell-surface biotinylation demonstrates that only natively glycosylated enzyme is delivered to the cell surface. COS cells were transfected with cysteine mutants representing each of the five phenotypes (as shown in Figure 2B). After biotinylation of cell-surface proteins with EZ-Link Sulfo-NHS-LC-Biotin and preparation of cell membranes, proteins were solubilized with Triton X-100 (100 000*g* supernatant) and incubated with streptavidin agarose beads. Biotinylated proteins were then eluted from streptavidin beads and analyzed by Western blotting using the KLH11 antibody. For each mutant and wild-type, lane E ("extract") is the Triton X-100 extract of NTPDase3 COS membranes before incubation with streptavidin beads and lane B ("bound") shows the protein which was bound to, and eluted from, the streptavidin beads. Total samples of wild-type NTPDase3 (T) were prepared by dissolving membranes in SDS loading buffer and are shown in lanes 1 and 14 for comparison. Putative disulfide bonds disrupted by cysteine mutations are indicated below the blot.

all *N*-glycans were removed by Endo H. This suggests that the lower band represents the partially glycosylated, high-mannose form of the protein residing in the ER. The middle band (marked with an arrowhead in Figure 4A, lane 6) was shifted by Endo H to the same degree as the wild-type protein, suggesting that this band represents the natively glycosylated protein that passed through the Golgi apparatus. As with the wild-type, the slight change in mobility caused by Endo H suggests that at least one of the N-glycosylation sites is high-mannose in structure, whereas the other glycosylation sites are of a complex state. The presence and properties of the upper-most band (marked with an asterisk in Figure 4A, lane 6) are unexpected. The apparent mass of this protein band is higher than that of wild-type, and it is not sensitive to Endo H, indicating that, in contrast to wild-type, this "hyper-glycosylated" molecular form does not contain high-mannose glycans.

All cysteine mutants were analyzed by treatment with Endo H, and representative mutants from each of the five phenotypic groups are shown in Figure 4B. The C347S mutant (with the fourth disulfide bond disrupted) was affected by Endo H in the same manner as the wild-type, indicating the native glycosylation of the protein (Figure 4B, lanes 8 and 9). In contrast, the electrophoretic mobility of the enzymatically inactive C289S mutant (with the third disulfide disrupted) was shifted to that of the core protein after treatment with Endo H, indicating the high-mannose form of immature protein residing in the ER. The other cysteine mutants are represented by two bands: the upper band of mature protein with complex glycans and the lower band of immature protein with high-mannose glycans (Figure 4B, lanes 4−7, 10, and 11). Endo H analysis revealed an identical pattern of glycosylation within each group of phenotypes (as defined in Figure 2B) and different glycosylation patterns between the groups (except the mutants with the second and the fifth disulfide disrupted, which do not differ in glycosylation). This further supports the assignment of disulfide bonds as shown in Figure 2C.

Effects of Cysteine Mutations on Trafficking of NTPDase3 to the Cell Surface. Deglycosylation analysis with Endo H revealed the detrimental effect of cysteine mutations, and consequent disruption of disulfide bonds on NTPDase3 glycosylation. Accumulation of immature proteins with high-mannose glycans suggests that the protein molecules failed to exit the ER and could not reach the cell surface. To clarify the effects of cysteine mutations on protein trafficking and delivery to the cell surface, we labeled the cell-surface proteins of the living, transfected COS cells with a membrane-impermeant reagent (Sulfo-NHS-LC-biotin). After solubilization of the cell membrane proteins, the biotinylated proteins were captured on streptavidin-agarose beads and analyzed by Western blotting with an antibody against NTPDase3 (Figure 5). Only the natively glycosylated, mature protein represented by the upper band was found to be captured by streptavidin beads and therefore delivered to the plasma membrane (Figure 5). In the C289S mutant that shows only immature glycosylation, no NTPDase3 protein was transported to the cell surface (Figure 5, compare lanes 8 and 9). In the C116S mutant, the biotinylated protein (Figure 5, lane 5) has slightly increased mass compared to wild-type-biotinylated protein (Figure 5, lane 3). This suggests that both natively glycosylated and hyperglycosylated molecular forms of the C116S mutant are delivered to the plasma membrane. Thus, cell-surface biotinylation experiments together with the deglycosylation analysis with Endo H strongly support the interpretation of electrophoretic phenotypes shown in Figures 2 and 3.

Sensitivity of C261S, C308S, and C261S/C308S Mutants to Reduction with DTT. The effect of DTT on ATPase activity was investigated for cysteine mutants having measurable enzymatic activity (Figure 6A). ATPase activities of all mutants, except C261S, C308S, and C261S/C308S,

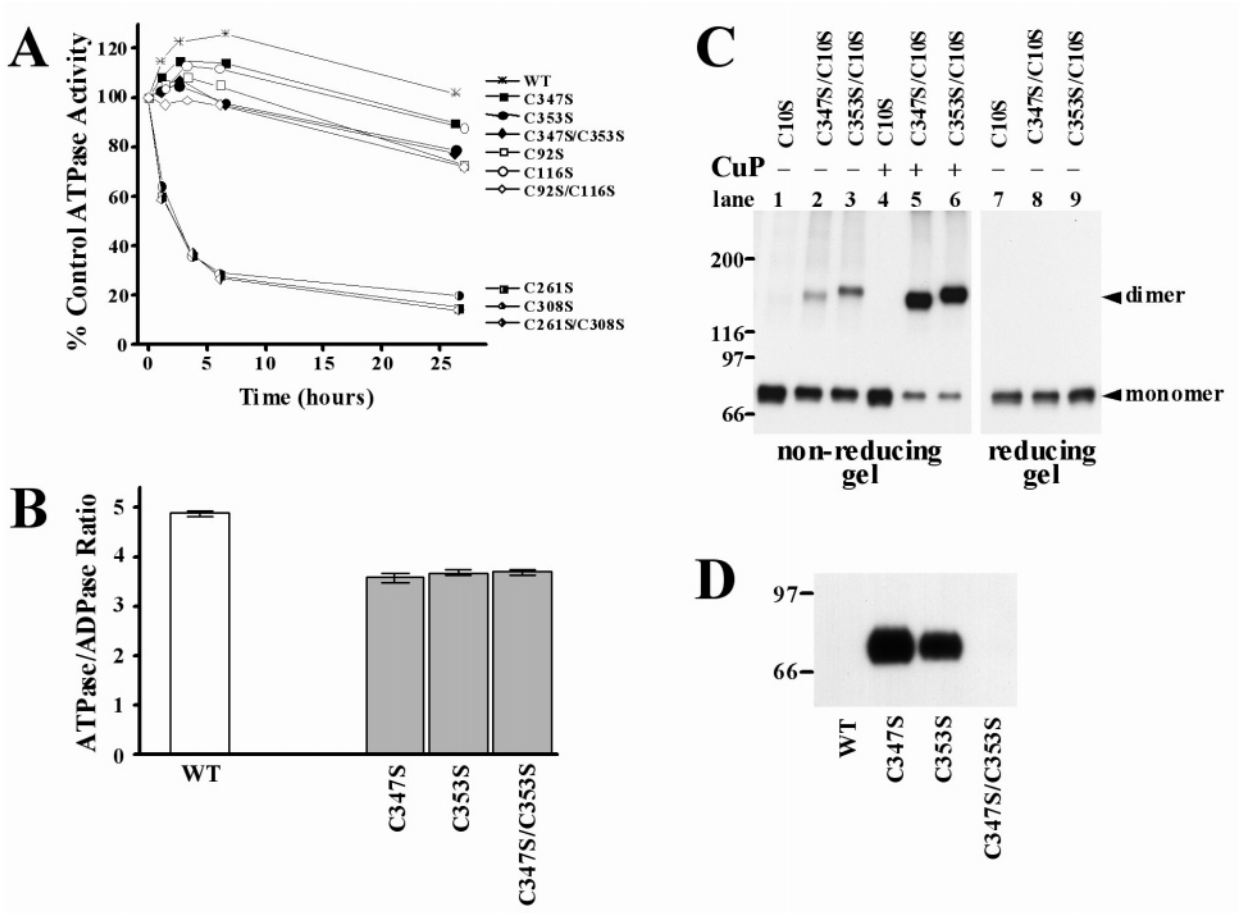

FIGURE 6: Specific effects of cysteine mutations that disrupt the 2nd and the 4th disulfide bonds. (A) Sensitivity of the ATPase activities of cysteine mutants to treatment with DTT. COS membranes transfected with wild-type and all cysteine mutants which retain residual enzymatic activity (see also Figure 2A) were treated with 10 mM DTT at 21 °C for various times before ATPase assay. Values represent the percentage of the activity of control samples incubated in parallel but without DTT. (B) Disruption of the putative C347−C353 disulfide results in a decrease in the ATPase/ADPase ratio. The experiment was performed with triplicate transfections for each mutant, using COS cells plated simultaneously in all dishes. ATPase and ADPase activities of membrane preparations were assayed, and the ATPase/ADPase ratios are presented as means ± SD of triplicate transfections. (C) C347S/C10S and C353S/C10S mutants form disulfide-linked dimers. C347S and C353S mutants were made in the background of the C10S NTPDase3 mutation that eliminates C10 in the cytoplasmic N-terminal tail and results in a fully active and wild-type-like enzyme (*55*). C10S mutation prevents spurious oxidative cross-linking of subunits via disulfide formation involving intracellular C10 which occurs to varying degrees during COS cell membrane preparation of wild-type NTPDase3 under nonreducing conditions (*55*). Membrane preparations treated with copper phenanthroline (CuP) and the control (nontreated) membrane preparations were subjected to SDS−PAGE in the absence of reducing agents to reveal the disulfide-linked dimers (lanes 1−6). Membranes were also analyzed by SDS−PAGE after reduction with DTT (lanes 7−9). The Western blots were probed with the KLH1 antibody. (D) Cell surface biotinylation with biotin-maleimide demonstrates the presence of free sulfhydryls in C347S and C353S mutants but not in wild-type and the C347S/C353S double mutant. After biotinylation of cell-surface proteins with sulfhydryl-specific reagent, biotin-maleimide, and preparation of cell membranes, proteins were solubilized with Triton X-100 (100 000*g* supernatant) and incubated with streptavidin agarose beads. Biotinylated proteins were then eluted from streptavidin beads and analyzed by Western blotting using the KLH1 antibody.

were above 70% of their respective controls after incubation for 24 h with 10 mM DTT at 21°C. Interestingly, the activity of wild-type and C10S NTPDase3 (data for C10S not shown) increased approximately 20−25% during the first 5 h of incubation. Several mutants also demonstrated a moderate increase in ATPase activity during this time period, but we could not correlate this increase with any mutation, nor could we provide any explanation for this reproducible phenomenon. In sharp contrast to the wild-type and other mutants, the ATPase activities of the mutants that disrupt the second disulfide bond (C261S, C308S, and C261S/C308S) were highly sensitive to reduction with DTT, decreasing to 50% after 2.5 h of incubation (Figure 6A). All three of these mutants showed an identical dependence of ATPase activity on DTT treatment. These identical phenotypic traits of single (C261S, C308S) and double (C261S/C308S) mutants strongly support the assignment of the second disulfide bond (C261−C308). Why are these mutants so different from others in their sensitivity to DTT? We hypothesize that due to an overlapping position of the second (C261−C308) and the third (C289−C334) disulfide bonds (Figure 2C), disruption of the second bond (C261−C308) increases the accessibility of the third bond (C289−C334) to DTT reduction. Since the disruption of the third bond (C289−C334) is incompatible with enzymatic activity, as evident from cysteine mutagenesis experiments (Figure 2), we hypothesize that disruption of this bond with DTT causes the same inactivation effect as the elimination of this bond by mutagenesis.

Additional Evidence That C347 and C353 are Disulfide-Paired. Mutagenic disruption of the fourth putative disulfide bond (C347−C353) had little effect on enzymatic activity, and no visible effect on glycosylation pattern. Therefore, we

looked for additional evidence whether these cysteine residues are paired in a disulfide bond or exist as free sulfhydryls, with the latter possibility being unlikely due to oxidative extracellular conditions and to the close proximity of these cysteines in the primary structure. We found that both single (C347S and C353S) and double (C347S/C353S) mutants have the same phenotypic trait, a decreased ATPase/ADPase ratio, which is statistically different from that of the wild-type (Figure 6B). This supports the assignment of the fourth disulfide bond (C347−C353) and argues against the possibility that these two cysteines exist as free sulfhydryls in NTPDase3.

Additional evidence for disulfide-pairing of C347 and C353 is presented in Figure 6C. C347S/C10S and C353S/C10S mutants form spontaneously disulfide-linked dimers that can be seen if SDS−PAGE is performed under nonreducing conditions (Figure 6C, lanes 2 and 3). The amount of dimers observed greatly increases after chemical oxidation with copper phenanthroline (Figure 6C, lanes 5 and 6). This oxidative cross-linking suggests the presence of an unpaired cysteine in the C347S/C10S and C353S/C10S mutants, but not in the C10S NTPDase3 used as a substitute for WT in this experiment. This further supports the pairing of C347 and C353 in a disulfide bond in the wild-type protein.

The disruption of the C347−C353 disulfide bond and the consequent appearance of an unpaired cysteine in C347S and C353S mutants were further demonstrated by cell surface biotinylation of living cells with a sulfhydryl-specific reagent, biotin-maleimide (Figure 6D). This reagent is not permeable to the plasma membrane under the conditions used, and therefore, it was used for labeling the accessible sulfhydryls in the extracellular part of NTPDase3. Both C347S and C353S showed strong labeling with biotin-maleimide, thus, indicating the presence of an accessible free sulfhydryl group in these mutants (Figure 6D). In contrast, the lack of labeling of wild-type and the C347S/C353S mutant demonstrates the absence of accessible unpaired cysteines in the extracellular parts on these proteins (Figure 6D). Taken together, the data presented in Figure 6B−D strongly support the conclusion that, in wild-type NTPDase3, C347 and C353 form a disulfide bond and do not exist as free sulfhydryls.

Acid Hydrolysis at the Unique Asp330−Pro331 Peptide Bond in NTPDase3. Protein aspartyl−prolyl peptide bonds are selectively cleaved under moderately acidic conditions (*44*, *45*). We took advantage of the presence of the single Asp330−Pro331 peptide bond in NTPDase3 (Figures 1 and 7A) to confirm the structure of disulfides near this site. Only the experiment with the C10S/C261S/C308S mutant is shown, although essentially identical results were obtained using C10S NTPDase3 that contains all native disulfide bonds (data not shown). The wild-type-like C10S mutant of NTPDase3 was used as a background for the reasons explained in the legend to Figure 6. The cysteines C261 and C308 were removed by mutation to demonstrate that neither of these cysteines participates in the disulfide bond connecting the two protein fragments produced after acid cleavage at Asp330−Pro331 (Figure 7A). A membrane preparation of transfected COS cells was solubilized with Triton X-100, and the supernatant (100 000*g*) was subjected to acid hydrolysis. As described above, Triton X-100 preferentially solubilizes the natively glycosylated enzyme and allows the removal of most of the immature partially glycosylated

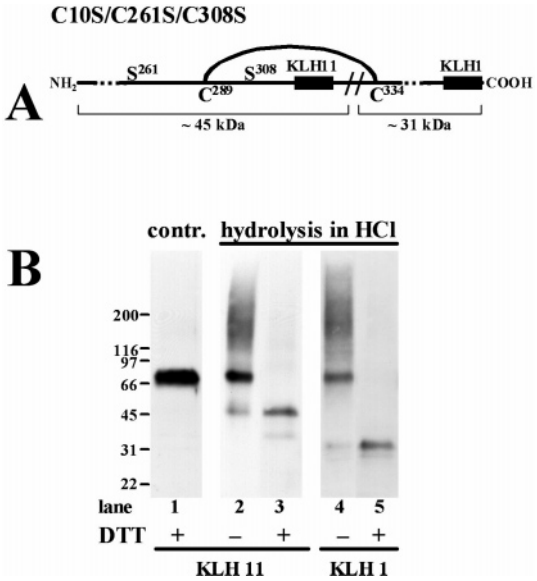

FIGURE 7: Limited acid hydrolysis at the unique Asp330−Pro331 peptide bond in NTPDase3 produces two fragments that are linked by a disulfide bond. The NTPDase3 double mutant C261S/C308S used in this experiment was made in C10S background for the reasons explained in the legend to Figure 6. (A) Schematic representation of NTPDase3 around the site of chemical cleavage. The Asp330−Pro331 cleavage site is depicted as //. The cleavage site is bridged by the putative C289−C334 disulfide bond (for additional features of the disulfide bond assignment, see Figures 1 and 2C). Cysteines C261 and C308 were eliminated by mutagenesis to demonstrate that neither of these cysteines is disulfide-paired with C334. Black boxes represent peptide epitopes recognized by two antibodies, KLH1 and KLH11. According to the disulfide assignments made in this work, the cleavage at the Asp330−Pro331 peptide bond is anticipated to produce two fragments of approximately 45 and 31 kDa that are linked together by the C289−C334 disulfide bond and can be separated by reduction of the disulfide. (B) C10S/C261S/C308S COS cell membranes were subjected to acid hydrolysis and analyzed by SDS−PAGE under both reducing (DTT+) and nonreducing (DTT-) conditions followed by Western blotting. The blots were probed with either the KLH1 antibody that recognizes a C-terminal epitope present in the 31 kDa fragment of NTPDase3 or with the KLH11 antibody that recognizes an internal epitope present in the 45 kDa fragment, as depicted in A. Lane 1 shows the mutant NTPDase3 after solubilization with Triton X-100 (100 000*g* supernatant), which was not subjected to acid hydrolysis (the control).

protein, which likely forms insoluble aggregates inside the cell. Accordingly, the supernatant is enriched in natively glycosylated protein band of approximately 80 kDa with no partially glycosylated protein or nonglycosylated core protein seen in the Western blot (Figure 7B, lane 1), the presence of which would complicate the interpretation of the results. Hydrolysis in 20 mM HCl for 17 h at 70 °C decreased the immunoreactivity of the major band, possibly due to partial nonspecific hydrolysis. However, most of the protein molecules were specifically cleaved at the Asp330−Pro331 site into two fragments that remained connected by a disulfide bond. After separation of these two fragments by reduction with DTT, the 80 kDa band disappears, and the protein fragments are recognized by the appropriate antibodies (∼45 kDa fragment is recognized by KLH11 and ∼31 kDa fragment is recognized by KLH1, Figure 7B). Small amounts of each fragment are seen under nonreducing conditions (i.e., ∼45 kDa fragment in Figure 7B, lane 2; ∼31 kDa fragment in Figure 7B, lane 4) suggesting that a small fraction of the disulfide bond connecting the two fragments was broken

during limited acid hydrolysis. These experiments indicate that the two fragments resulting from cleavage of NTPDase3 at the Asp330−Pro331 site are connected by a disulfide bond, and that neither C261 nor C308 are involved in that disulfide. This is consistent with the assignment of disulfide bonds shown in Figure 2C.

Computational Modeling of NTPDase3. Several Psi-BLAST iterations revealed a weak sequence similarity of the extracellular sequence of NTPDase3 to multiple members of the exopolyphosphatase/guanosine pentaphosphate phosphohydrolase (PPX/GPPA) family. In addition, the N-terminal fragment of the extracellular portion of NTPDase3 (residues 61−229) was aligned by Psi-BLAST to a fragment of structurally resolved bacterial PPX/GPPA protein (Protein Data Bank code 1T6C, chain A) with the E-value of 0.002 and a sequence identity of 14%. Using the FUGUE and FFAS fold recognition servers, we also identified the 3-D structure of the recently crystallized bacterial PPX/GPPA enzyme (PDB code 1T6C (*17*)) as the only protein with significant structural similarity to the extracellular portion of NTPDase3. For example, the FUGUE server matched NTPDase3 with the 1T6C template with a Z-score of 12.3, which corresponds to over 99% confidence level of the two proteins having similar structural folds (a "certain" match). The FFAS match into the 1T6C template is also highly confident. We then used homology modeling and the SCWRL server to obtain putative models of the NTPDase3 structure based on the FUGUE and FFAS alignments (the alignment and model generated by the FUGUE program are shown in Figure 8B and 8C, respectively, while the alignment, model, and coordinates generated by the FFAS program are included as files in the Supporting Information). The main differences between the FUGUE and FFAS alignments and the resulting models involve the central fragment (residues from approximately 240 to 380, indicated by a dashed box in Figure 8B), a region which was also identified as a putative independent domain by the PRODOM server (version available from the Predict Protein server; see Materials and Methods).

For further validation of the predicted structural similarity between NTPDases and PPX/GPPA families, we generated secondary structure and solvent accessibility predictions for NTPDase3 using PsiPRED, SABLE, and PROFsec programs, to compare these predictions with the template PPX/GPPA protein. These predictions were found to be largely consistent with each other and with the proposed structural homologue PPX/GPPA (see Figure 8B for the secondary structure comparisons), except for the central fragment of the extracellular domain involving NTPDase3 residues from approximately 240 to 380 (indicated by a dashed box in Figure 8B), where again the predictions and the template do not match. Therefore, we performed additional fold recognition searches using this approximately 240−380 NTPDase3 sequence fragment as a query sequence and obtained, using LOOPP and 3D-PSSM servers, a number of weak matches to a tyrosine phosphatase and other structurally related proteins. In particular, LOOPP matched this domain with the structure of a tyrosine phosphatase (PDB code 1P8A). The resulting amino acid alignment and a model showing the 6 NTPDase3 cysteines (filename = LOOPP_1P8A_NTPDase3_domain_alignment_and_model.jpg), as well as the PDB structure file (coordinates) generated using this tyrosine phosphatase as template for this NTPDase3 domain (filename = LOOPP_1P8A_NTPDase3_inner_domain_coordinates.pdb) are included in the Supporting Information.

DISCUSSION

Disulfide bonds play essential roles in folding, maturation, stability, and function of certain proteins and are frequently found in extracellular proteins (*37*, *46*−*48*). The conservation of 10 cysteines in the extracellular regions of cell-surface NTPDases suggests their participation in the formation of disulfide bonds and the importance of these bonds for the structure and function of the enzymes. As essential structural determinants, disulfide bonds define the regions in the primary protein structure that are in proximity to each other in the 3-D structure. Thus, the knowledge of disulfide bond arrangement is helpful for both constructing the 3-D models and for validation of the accuracy of the models. Therefore, we are interested in identifying the disulfide bonds in NTPDases and using this information for structural modeling.

We have recently determined the disulfide pairing of the four conserved cysteine residues in the bacterially expressed soluble NTPDase6 using chemical techniques (*3*). Preliminary attempts to use the same methodology to determine the disulfide bonds in membrane-bound NTPDases were not successful due to the increased complexity of the system (the membrane-bound enzymes have 10 conserved extracellular cysteines and therefore, presumably, five conserved disulfide bonds, compared to two disulfides in the soluble NTPDase6) and the limited availability of pure membrane-bound NTPDase proteins. Therefore, we used a cysteine mutagenesis approach to characterize the disulfide bonds in the membrane-bound NTPDase3. This technique has been used in many systems to identify the location of disulfides and to confirm the disulfide bonds determined by protein chemistry techniques (*9*−*15*, *49*). The disruption of a disulfide bond by cysteine mutagenesis is expected to cause a similar effect on the structure and function of the protein regardless whether one or both cysteines within the same disulfide bond are mutated. In contrast, double cysteine mutations that disrupt two disulfide bonds are expected to be more harmful to the protein structure and function than the respective single mutations. In agreement with this principle, we found that the 15 cysteine mutants of NTPDase3 could be arranged into five distinct groups according to their nucleotidase activities and glycosylation patterns, suggesting the existence of the disulfide bonds depicted in Figures 2C and 8A. This disulfide architecture is strongly supported by the observation that the double cysteine mutations disrupting two putative disulfide bonds differ in phenotypes from single or double mutations that disrupt one disulfide bond (Figure 3).

The proposed disulfide bond pattern was further confirmed by the identification of unique phenotypic traits associated with elimination of each of the putative disulfides. Thus, disruption of the first disulfide (mutations C92S, C116S, C92S/C116S) caused the appearance of a hyperglycosylated protein (Figure 4A, lane 6, and Figure 4B, lane 2). This glycoform lost sensitivity to Endo H compared to the wild-type, suggesting the abnormal terminal glycosylation of an *N*-glycan chain, which in the wild-type is likely shielded from terminal processing and is high-mannose in structure. The

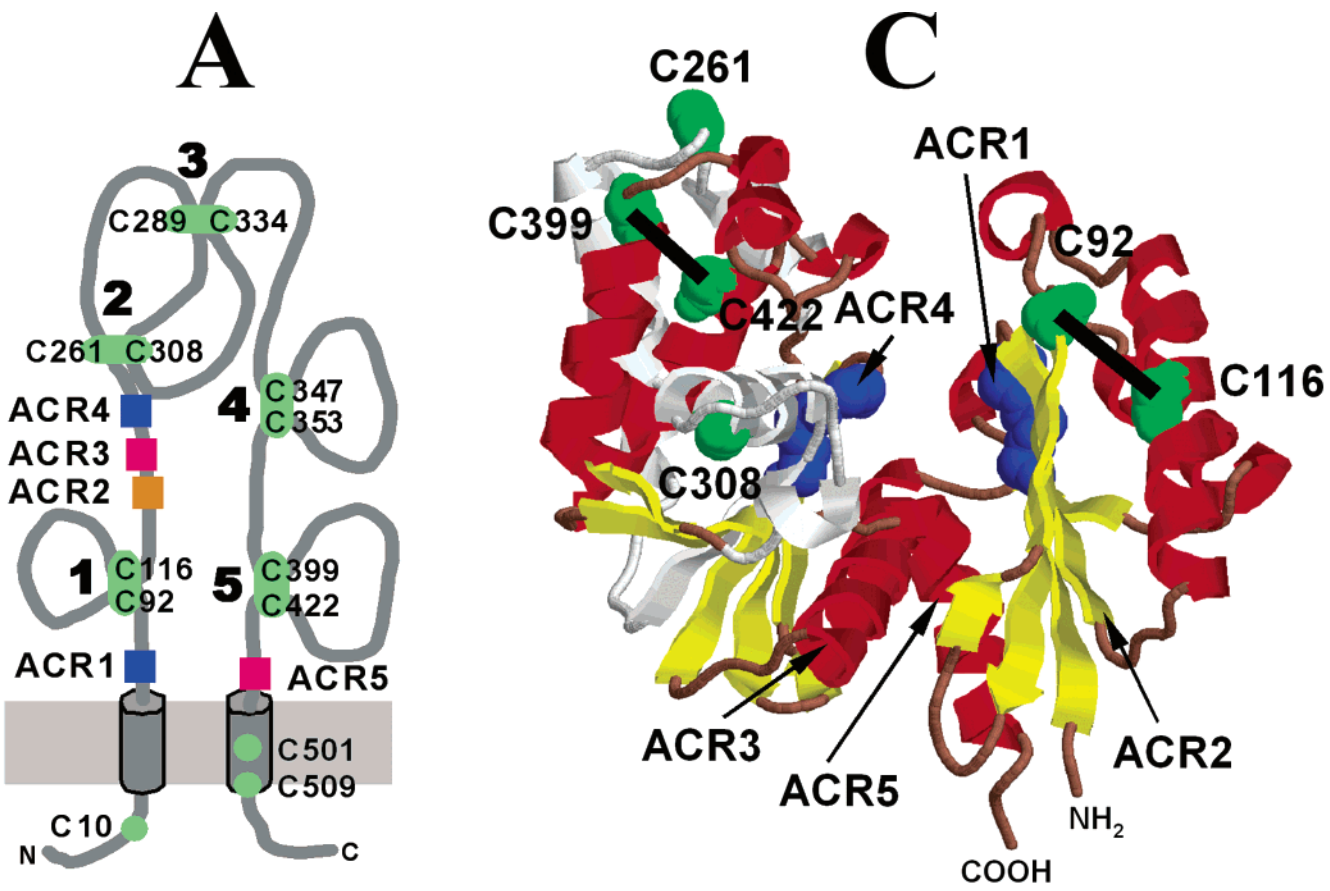
A
3
C289 C334
2
C261 C308
ACR4
ACR3
ACR2
4
C347
C353
1
C116
C92
5
C399
C422
ACR1
ACR5
C501
C509
C10
N
C
C
C261
C399
ACR1
C92
C422
ACR4
C116
C308
ACR3
ACR5
ACR2
NH2
COOH

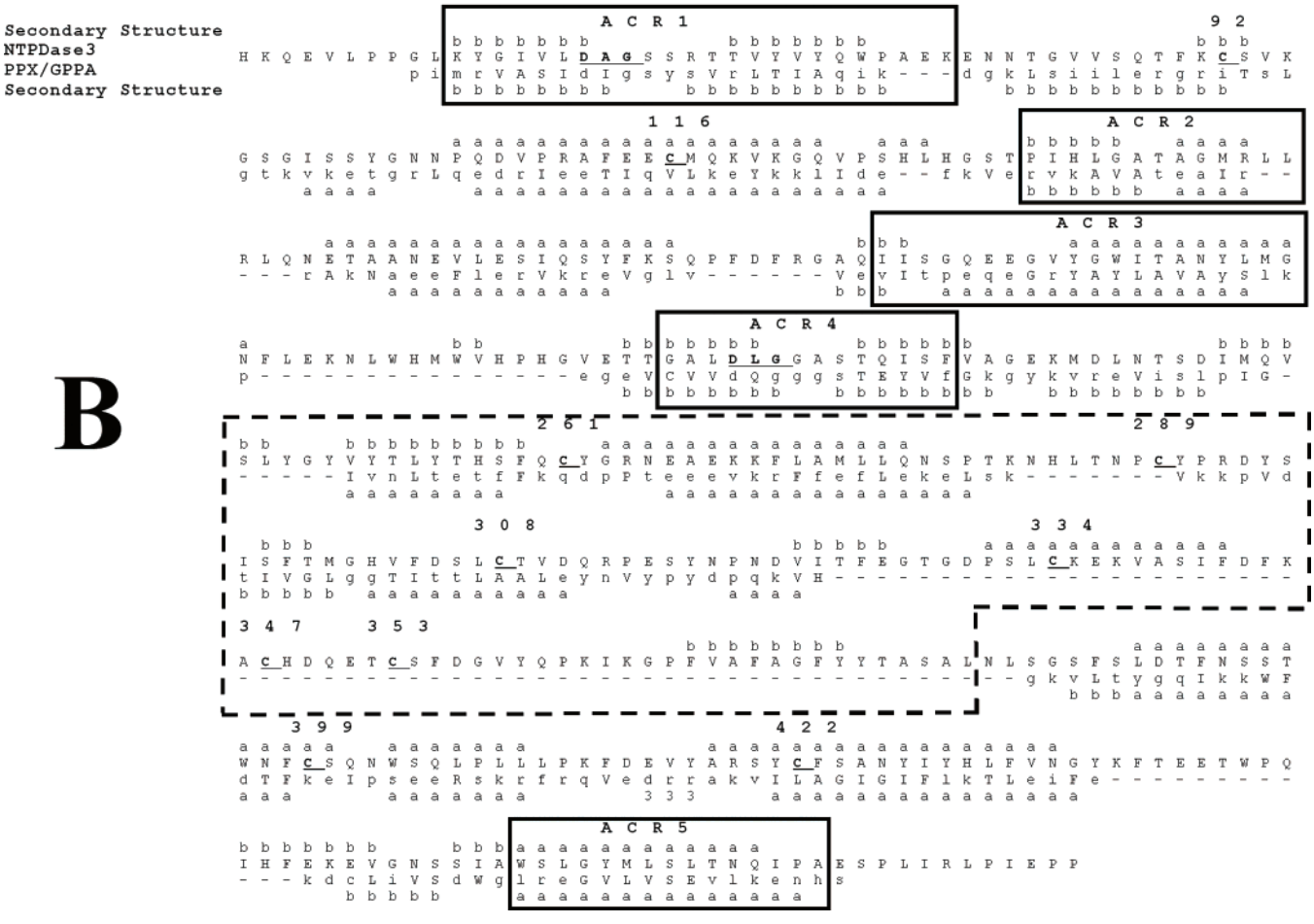
B
Secondary Structure
NTPDase3
PPX/GPPA
Secondary Structure
ACR1
ACR2
ACR3
ACR4
ACR5

FIGURE 8: Models of NTPDase3. (A) A cartoon representation of the entire NTPDase3 protein, showing in green the location of the three unpaired cysteines (C10, C501, and C509), as well as the locations of five disulfide bonds formed by 10 extracellular cysteines. The apyrase conserved regions (ACRs) are also depicted, using the same color scheme as shown in the 3-D model in panel C. The N- and C-terminal transmembrane helices are shown as dark gray cylinders, and the cytoplasmic N- and C-termini are also indicated. (B) Sequence alignment of the extracellular region of NTPDase3 (residues 46−485) with the exopolyphosphatase/guanosine pentaphosphate phosphohydrolase sequence (PPX/GPPA, PDB code 1T6C (*17*)), generated by the protein fold recognition program, FUGUE. The top line is the SABLE server-predicted secondary structure for NTPDase3. The NTPDase3 sequence is shown in the second line in upper case letters. For the PPX/GPPA sequence shown in line 3 below the NTPDase3 sequence, solvent accessible residues are represented by lower case letters, while solvent inaccessible residues are represented by upper case letters. Gaps in the alignment are indicated by dashes (−). The PPX/GPPA secondary structure is shown in line 4: "a" for α-helix, "b" for β-sheet, and "3" for 3_{10} helix. The NTPDase3 apyrase conserved regions (ACRs) are defined as residues having a PLOT SIMILARITY (part of the SeqWeb suite of analysis programs) multiple sequence alignment score of >2.0 (see Figure 7 in ref *56*)) and are boxed and labeled above the NTPDase3 sequence. The "DXG" phosphate binding motifs of NTPDase3 are bolded and underlined in ACR1 and ACR4. The 10 extracellular cysteines involved in five disulfide bonds are bolded and underlined, with the NTPDase3 residue number for each cysteine shown above the sequence. The part of the sequence exhibiting poor fold similarity to the PPX/GPPA protein is indicated by a dashed box. (C) The 3-D model of the extracellular region of NTPDase3 generated by the FUGUE program based on the PPX/GPPA structure. The model consists of the peptide backbone only and does not contain the amino acid side chains. Helixes are represented by red ribbons and beta sheets by yellow arrows, while turns and coils are colored brown, except for the part of the model exhibiting poor fold similarity to the PPX/GPPA protein, which is indicated in white and gray regardless of secondary structure. The backbone locations of the NTPDase3 cysteine residues are indicated in the model by space-filling mode (green), as are the "DXG" motifs found in ACR1 and ACR4 (blue). Although the model does not include the backbone positions for all 10 cysteines (due to gaps in the alignment, see panel B), the backbone positions of cysteines 92 and 116 (first disulfide), as well as cysteines 399 and 422 (fifth disulfide), are in close proximity (indicated by black bars), thus, confirming the accuracy of the parts of the model containing these cysteines. Cysteines 261 and 308 (second disulfide) are located far apart in the model, suggesting that the folding pattern in this part of the model is not correct, since this is not compatible with the existence of a C261−C308 disulfide bond. Also of note are the locations of ACR3 and ACR5 in the model; they each constitute an alpha helix, serving as the connectors between the two lobe domains that make up the active site: the N-terminal domain containing ACR1, and the C-terminal domain containing ACR4. The putative active site is located in the cleft between ACR1 and ACR4.

unique feature of mutations that eliminate the second putative disulfide (C261S, C308S, C261S/C308S) is the remarkable sensitivity of the residual ATPase activity to reduction with DTT (Figure 6A). The elimination of the third putative disulfide (C289S, C334S, C289S/C334S) resulted in the unique glycosylation pattern represented only by the immature, high-mannose glycoprotein that resides in the ER and failed to reach the cell surface (Figure 4B, lanes 6 and 7, and Figure 5, lanes 8 and 9). The specific phenotypic trait associated with elimination of the fourth putative disulfide bond (mutations C347S, C353S, C347S/C353S) is the decrease in ATPase/ADPase ratio, as shown in Figure 6B. Although disruption of the fifth putative disulfide (mutations C399S, C422S, C399S/C422S) caused total inactivation of the enzyme (Figure 2A), the mutants show some amount of apparently natively glycosylated NTPDase3 that is delivered to the cell surface (Figure 4B, lanes 10 and 11, and Figure 5, lanes 12 and 13). This specific feature suggests that the elimination of the fifth putative disulfide may not severely deteriorate the global protein conformation, allowing some enzyme molecules to pass through the protein folding quality control mechanisms operating in the ER (*48*) and to undergo native terminal glycosylation in the Golgi. Taken as a whole, these additional phenotypic traits, uniquely associated with elimination of each of the putative disulfides by either single or double cysteine mutations, confirm the disulfide bond assignments originally deduced from the enzymatic activity and glycosylation phenotypes (Figure 2).

The identified disulfide bonds are of differential importance for the processing, trafficking, and enzymatic activity of NTPDase3. The third bond (C289−C334) and the fifth bond (C399−C422) are essential, since their disruption by cysteine mutagenesis resulted in completely inactive enzymes. These two disulfide bonds are equivalent to two disulfides determined in the soluble NTPDase6 (*3*). The fourth disulfide (C347−C353) is not essential, since disruption of this bond only slightly decreases the preferential hydrolysis of ATP versus ADP, while the first (C92−C116) and the second (C261−C308) disulfides are of intermediate importance for processing and enzymatic activity of NTPDase3.

Because of the currently insurmountable obstacles for the experimental determination of the 3-D structure of membrane-bound NTPDases, we are interested in computational comparative modeling of these enzymes. We reasoned that the knowledge of disulfide structure could assist in building, refining, and validating such computational models. We used sequence alignment and fold recognition methods to identify putative homologues and build structural models of NTPDase3 and other related NTPDases. We found a weak sequence similarity of the extracellular sequence of NTPDase3 to multiple members of the exopolyphosphatase/guanosine pentaphosphate phosphohydrolase (PPX/GPPA) family. Using the FUGUE and FFAS fold recognition servers, we also identified the 3D structure of the recently crystallized bacterial PPX/GPPA enzyme (*17*) as the only protein with significant structural similarity to the extracellular portion of NTPDase3. The FUGUE program matches sequences with structures using sequence as well as local structural environment information and structure-dependent gap penalties (*27*). The FFAS server relies, in turn, on matching multiple sequence alignment profiles, as encoded by the Position Specific Substitution Matrices obtained using Psi-BLAST (*28*). Therefore, the fact that these two different approaches result in very similar alignments adds confidence to the prediction.

The peptide backbone of one NTPDase3 model, based on the FUGUE alignment in Figure 8B, is presented in Figure 8C (the sequence alignment and its corresponding model based on the FFAS analysis of the extracellular sequence of NTPDase3 are similar to those generated by FUGUE and are included in the Supporting Information). For the amino acid residues in the extracellular portion of NTPDase3 that do not have corresponding residues in the template structure of PPX/GPPA, gaps are inserted in the sequence alignment by the FUGUE program (Figure 8B), and no backbone

coordinates are predicted in the 3-D model. The gaps are extensive, especially in the middle part of the sequence, causing four NTPDase3 cysteines (C289, C334, C347, and C353, corresponding to the third and fourth disulfides) to be absent from the 3-D model. Thus, the 3-D structure built by FUGUE (Figure 8C) is a rough model of NTPDase3. However, it is the first available 3-D model of an NTPDase with a high confidence of having structural folds similar to those in a protein (PPX/GPPA) whose 3-D structure has been determined. In addition, there are several pieces of evidence that support the quality of the sequence alignment and the confidence of the structural homology recognition used to generate the model in Figure 8C.

First, there are similarities in general biochemical properties of NTPDases and the PPX/GPPA enzymes. Both have been recognized to belong to a superfamily of enzymes characterized by the actin-like ATPase domain (*17*, *18*, *50*−*52*), which contain the phosphate 1 and phosphate 2 motifs that have strictly conserved DXG residues. NTPDases have apyrase-conserved regions analogous to these sequences (ACR1 and ACR4), and mutagenic analyses of DXG residues in these ACRs have confirmed their critical importance for enzymatic activity and thus their homology with the actin superfamily (*18*). In addition, the enzymatic activities of NTPDases and PPXGPPA depend on divalent cations, and a calcium-binding site was identified in the crystal structure of PPX/GPPA in a sequence homologous to ACR4 of NTPDase3 (*17*).

Second, visual inspection of the N-terminal and C-terminal parts of the sequence alignment (Figure 8B, the sequence alignment above and below the dashed box) reveals many matches between the predicted secondary structural elements of NTPDase3 and the experimentally determined secondary structure in the PPX/GPPA crystals (Figure 8B), as well as only short fragments in the sequence of NTPDase3 (shown as the gaps in PPX/GPPA sequence) that are not represented in the NTPDase3 3-D model. This suggests that the N-terminal part of the NTPDase3 model, including ACR1, ACR2, and ACR3, which constitutes the whole N-terminal lobe of the 3-D structure (the lobe shown on the right side in Figure 8C), as well as ACR4 and the C-terminal part that includes C399, C422, and ACR5, may be well-modeled. Conversely, the middle part of the NTPDase3 sequence containing six cysteines (C261, C289, C308, C334, C347, and C353, corresponding to the second, third, and fourth disulfide bonds, respectively) is interrupted by long fragments that are not represented in the 3-D model, thus likely causing significant deviations of the model in this region from the real structure. In addition to visual inspection, we used the program Verify3D to evaluate the fitness of various parts of NTPDase3 to the model obtained by FUGUE. This analysis revealed that the highest scores (and therefore the highest probability of the model being accurate) are in the parts of the model corresponding to ACR1, ACR2, ACR3, and ACR4, in addition to the part near the extreme C-terminus containing ACR5 (see file 3 in Supporting Information). The Verify3D analysis also suggests low confidence for the middle parts of the model that contain 4 cysteines (C261, C308, C399, C422, corresponding to the second and fifth disulfides) and that are interrupted by long nonrepresented fragments including 4 cysteines (C289, C334, C347, C353, corresponding to the third and fourth disulfides).

Third, we used the identified disulfide structure of NTPDase3 as a criterion for evaluation of the correctness of the different parts of the model. We reasoned that, in the correct 3-D structure, the regions in the sequence that are connected by a disulfide bond should be positioned close to each other. As shown in Figure 8B,C, only 6 (C92, C116, C261, C308, C399, and C422) out of 10 conserved extracellular cysteines are represented in the model, and the other four cysteines have no corresponding residues in the template structure of PPX/GPPA. Cysteines within the first disulfide bond (C92, C116) and fifth disulfide bond (C399, C422) are located in proximity to each other in the model (Figure 8C; note that only backbone atoms are indicated in green space filling mode, with no side chains included), thus, suggesting that the 3-D model in these parts is compatible with the formation of disulfide bonds 1 and 5. In contrast, C261 and C308 (second disulfide) are located far apart in the model, suggesting that the folding pattern in this part of the model is not compatible with the existence of disulfide bond 2 and, consequently, is not correct. This observation further supports the notion that the initial part of the NTPDase3 sequence (from ACR1 to ACR3, as well as ACR4) and the terminal part (from C399 to ACR5) are likely well-modeled, whereas the modeling of the middle part is not likely to correctly represent the real structure of NTPDase3. Given the overlapping arrangement of the second (C261−C308) and third (C289−C334) disulfide bonds (Figure 8A) in NTPDase3, it seems unlikely that the correct spatial positioning of C261 and C308 may occur without the presence of the third disulfide bond (C289−C334), which is not represented in the model.

As described in the Results section, the main differences between the model of NTPDase3 based on the FUGUE alignment versus the model based on the FFAS alignment involve the central fragment (residues from approximately 240−380). Fold recognition searches using this putative independent domain as a query sequence revealed a number of weak matches to a tyrosine phosphatase and other structurally related proteins. Interestingly, the model based on the weak homology of this domain with the tyrosine phosphatase (PDB code 1P8A) did place the six NTPDase3 cysteines in positions consistent with the second (C261−C308), third (C289−C334), and fourth (C347−C355) disulfide bonds (see Supporting Information, LOOPP_1P8A_NTPDase3_domain_alignment_and_model.jpg). Thus, the identified disulfide structure aids in the evaluation of the generated 3-D models of NTPDase3 and will be instrumental in further refinements and validation of these and other models.

The 3-D model of the extracellular portion of NTPDase3 suggests the structural basis for the importance of several ACRs for the nucleotidase activities of the NTPDases. ACR1 and ACR4 are each represented by a β-hairpin loop located on either side of a large cleft forming the active site (as highlighted in Figure 8C by showing the highly conserved DXG sequences within ACR1 and ACR4 in blue space filling mode). ACR3 and ACR5 precisely correspond to two α-helices that connect the N- and C-domains (see Figure 8B,C). Such a structure allows significant rotational movements of the domains relative to one another, which have been described for the enzymes of the actin-like ATPase domain superfamily as a "butterfly-like" opening of the active

site cleft involved in catalysis (*50*, *53*). Although such extracellular domain motions have not been described yet for membrane-bound NTPDases, Grinthal and Guidotti reported significant ATP-dependent changes in the relative position of two transmembrane domains flanking the extracellular region of NTPDase1 (*54*). It is logical to hypothesize that these changes in position and orientation of the transmembrane domains may correlate with, and possibly be functionally linked to, the "butterfly-like" movements of the extracellular domains, which are presumably needed for nucleotide hydrolysis.

In summary, we have used site-directed mutagenesis to define the positions and importance of the five conserved extracellular disulfide bonds in NTPDase3. The locations of some of these disulfide bonds have been used to validate, in part, newly generated 3-D models of the extracellular portion of NTPDase3. The usefulness and validity of these 3-D models is supported by the finding that FUGUE modeling of the extracellular sequences of all of the known cell-surface and soluble NTPDases (1−3, 5−6, and 8) gave essentially the same result, that is, identification of the PPX/GPPA protein as the lone structure with significant fold similarity to NTPDases and generation of theoretical 3-D models that look, in all cases, very similar to the NTPDase3 model (see NTPDase_FUGUE_Models.jpg in the Supporting Information). The NTPDase3 model defines the structural basis for the importance of the five apyrase-conserved regions (ACRs). This model is a starting point for future experimentation and 3-D model refinement for the purpose of defining the nucleotide and divalent cation binding sites, as well as for probing the hydrolytic mechanisms and nucleotide specificities of the NTPDases.

ACKNOWLEDGMENT

We thank Megan Strouth for her assistance in mutagenesis, transfection, and deglycosylation experiments during her student laboratory rotation. We also thank Dr. Saswata Basu for providing C10S mutant NTPDase3 COS cell membranes and Maria Ivanenkov for her assistance in preparation of COS cell membranes.

SUPPORTING INFORMATION AVAILABLE

The following eight files constitute the Supporting Information submitted as documentation of the threading and homology modeling part of this study. This material is available free of charge via the Internet at http://pubs.acs.org.

1. "FUGUE_NTPDase3_3D_coordinates.pdb" is the FUGUE-generated NTPDase3 3-D model coordinates based on template 1T6C (without side chains).

2. "FUGUE_NTPDase3_3D_coordinates_with_side_chains.pdb" is the FUGUE-generated NTPDase3 3-D model coordinates based on template 1T6C (with side chains).

3. "Verify3D_NTPDase3_FUGUE_Model.jpg" is the annotated Verify3D analysis of the FUGUE NTPDase3 3-D model (based on analysis of Supporting Information file 1, without side chains).

4. "FFAS_NTPDase3_alignment_and_model.jpg" is the FFAS-generated NTPDase3 amino acid alignment and 3-D model representation (similar to Figure 8B,C) based on template 1T6C.

5. "FFAS_NTPDase3_3D_coordinates_with_side_chains.pdb" is the FFAS-generated NTPDase3 3-D model coordinates based on template 1T6C (with side chains).

6. "LOOPP_1P8A_NTPDase3_domain_alignment_and_model.jpg" is the LOOPP-generated NTPDase3 amino acid alignment and representation of the LOOPP-generated 3-D model of the approximately 240−380 domain of NTPDase3 (similar in format to Figure 8B,C), based on the template tyrosine phosphatase structure (PDB 1P8A).

7. "LOOPP_1P8A_NTPDase3_inner_domain_coordinates.pdb" is the LOOPP-generated 3-D model coordinates of the approximately 240−380 domain of NTPDase3 using the tyrosine phosphatase (PDB 1P8A) structure as a template.

8. "NTPDase_FUGUE_Models.jpg" is the representation of FUGUE-generated 3-D models of NTPDases1−3, 5, 6, and 8, all based on template 1T6C (similar to Figure 8C for NTPDase3).

REFERENCES

1. Zimmermann, H. (1999) Two novel families of ectonucleotidases: molecular structures, catalytic properties and a search for function, *Trends Pharmacol. Sci. 20*, 231−236.
2. Plesner, L. (1995) Ecto-ATPases: identities and functions, *Int. Rev. Cytol. 158*, 141−214.
3. Ivanenkov, V. V., Murphy-Piedmonte, D. M., and Kirley, T. L. (2003) Bacterial expression, characterization, and disulfide bond determination of soluble human NTPDase6 (CD39L2) nucleotidase: implications for structure and function, *Biochemistry 42*, 11726−11735.
4. Murphy-Piedmonte, D. M., Crawford, P. A., and Kirley, T. L. (2005) Bacterial expression, folding, purification and characterization of soluble NTPDase5 (CD39L4) Ecto-nucleotidase, *Biochim. Biophys. Acta 1747*, 251−259.
5. Dai, J., Liu, J., Deng, Y., Smith, T. M., and Lu, M. (2004) Structure and protein design of a human platelet function inhibitor, *Cell 116*, 649−659.
6. Smith, T. M., Hicks-Berger, C. A., Kim, S., and Kirley, T. L. (2002) Cloning, expression, and characterization of a soluble calcium-activated nucleotidase, a human enzyme belonging to a new family of extracellular nucleotidases, *Arch. Biochem. Biophys. 406*, 105−115.
7. Murphy, D. M., Ivanenkov, V. V., and Kirley, T. L. (2003) Bacterial expression and characterization of a novel, soluble, calcium binding and calcium activated human nucleotidase, *Biochemistry 42*, 2412−2421.
8. Yang, M., and Kirley, T. L. (2004) Site-directed mutagenesis of human soluble calcium-activated nucleotidase 1 (hSCAN-1): identification of residues essential for enzyme activity and the Ca(2+)-induced conformational change, *Biochemistry 43*, 9185−9194.
9. Noda, K., Saad, Y., Graham, R. M., and Karnik, S. S. (1994) The high affinity state of the beta 2-adrenergic receptor requires unique interaction between conserved and non-conserved extracellular loop cysteines, *J. Biol. Chem. 269*, 6743−6752.
10. Wendland, M., von Figura, K., and Pohlmann, R. (1991) Mutational analysis of disulfide bridges in the Mr 46,000 mannose 6-phosphate receptor. Localization and role for ligand binding, *J. Biol. Chem. 266*, 7132−7136.
11. Heerding, J. N., Hines, J., Fluharty, S. J., and Yee, D. K. (2001) Identification and function of disulfide bridges in the extracellular domains of the angiotensin II type 2 receptor, *Biochemistry 40*, 8369−8377.
12. Ohyama, K., Yamano, Y., Sano, T., Nakagomi, Y., Hamakubo, T., Morishima, I., and Inagami, T. (1995) Disulfide bridges in extracellular domains of angiotensin II receptor type IA, *Regul. Pept. 57*, 141−147.
13. Long, D., Wilcox, W. C., Abrams, W. R., Cohen, G. H., and Eisenberg, R. J. (1992) Disulfide bond structure of glycoprotein D of herpes simplex virus types 1 and 2, *J. Virol. 66*, 6668−6685.
14. Deng, P., Wang, Y. L., Pattengale, P. K., and Rettenmier, C. W. (1996) The role of individual cysteine residues in the processing,

structure, and function of human macrophage colony-stimulating factor, *Biochem. Biophys. Res. Commun. 228*, 557−566.
15. Ennion, S. J., and Evans, R. J. (2002) Conserved cysteine residues in the extracellular loop of the human P2X(1) receptor form disulfide bonds and are involved in receptor trafficking to the cell surface, *Mol. Pharmacol. 61*, 303−311.
16. Clyne, J. D., Wang, L. F., and Hume, R. I. (2002) Mutational analysis of the conserved cysteines of the rat P_2X_2 purinoceptor, *J. Neurosci. 22*, 3873−3880.
17. Kristensen, O., Laurberg, M., Liljas, A., Kastrup, J. S., and Gajhede, M. (2004) Structural characterization of the stringent response related exopolyphosphatase/guanosine pentaphosphate phosphohydrolase protein family, *Biochemistry 43*, 8894−8900.
18. Smith, T. M., and Kirley, T. L. (1999) Site-directed mutagenesis of a human brain ecto-apyrase: evidence that the E-type ATPases are related to the actin/heat shock 70/sugar kinase superfamily, *Biochemistry 38*, 321−328.
19. Smith, T. M., and Kirley, T. L. (1998) Cloning, sequencing, and expression of a human brain ecto-apyrase related to both the ecto-ATPases and CD39 ecto-apyrases, *Biochim. Biophys. Acta 1386*, 65−78.
20. Stoscheck, C. M. (1990) Increased uniformity in the response of the coomassie blue G protein assay to different proteins, *Anal. Biochem. 184*, 111−116.
21. Fiske, C. H., and Subbarow, Y. (1925) The colorometric determination of phosphorous, *J. Biol. Chem. 66*, 375−400.
22. Smith, T. M., and Kirley, T. L. (1999) Glycosylation is essential for functional expression of a human brain ecto-apyrase, *Biochemistry 38*, 1509−1516.
23. Emini, E. A., Hughes, J. V., Perlow, D. S., and Boger, J. (1985) Induction of hepatitis A virus-neutralizing antibody by a virus-specific synthetic peptide, *J. Virol. 55*, 836−839.
24. Careaga, C. L., and Falke, J. J. (1992) Thermal motions of surface alpha-helices in the D-galactose chemosensory receptor. Detection by disulfide trapping, *J. Mol. Biol. 226*, 1219−1235.
25. Altschul, S. F., Madden, T. L., Schaffer, A. A., Zhang, J., Zhang, Z., Miller, W., and Lipman, D. J. (1997) Gapped BLAST and PSI-BLAST: a new generation of protein database search programs, *Nucleic Acids Res. 25*, 3389−3402.
26. Fischer, D., Elofsson, A., Rychlewski, L., Pazos, F., Valencia, A., Rost, B., Ortiz, A. R., and Dunbrack, R. L., Jr. (2001) CAFASP2: the second critical assessment of fully automated structure prediction methods, *Proteins* (Suppl. 5) 171−183.
27. Shi, J., Blundell, T. L., and Mizuguchi, K. (2001) FUGUE: sequence-structure homology recognition using environment-specific substitution tables and structure-dependent gap penalties, *J. Mol. Biol. 310*, 243−257.
28. Rychlewski, L., Jaroszewski, L., Li, W., and Godzik, A. (2000) Comparison of sequence profiles. Strategies for structural predictions using sequence information, *Protein Sci. 9*, 232−241.
29. Jones, D. T. (1999) Protein secondary structure prediction based on position-specific scoring matrices, *J. Mol. Biol. 292*, 195−202.
30. Adamczak, R., Porollo, A., and Meller, J. (2004) Accurate prediction of solvent accessibility using neural networks-based regression, *Proteins 56*, 753−767.
31. Canutescu, A. A., Shelenkov, A. A., and Dunbrack, R. L., Jr. (2003) A graph-theory algorithm for rapid protein side-chain prediction, *Protein Sci. 12*, 2001−2014.
32. Meller, J., and Elber, R. (2001) Linear programming optimization and a double statistical filter for protein threading protocols, *Proteins 45*, 241−261.
33. Kelley, L. A., MacCallum, R. M., and Sternberg, M. J. (2000) Enhanced genome annotation using structural profiles in the program 3D-PSSM, *J. Mol. Biol. 299*, 499−520.
34. Bowie, J. U., Luthy, R., and Eisenberg, D. (1991) A method to identify protein sequences that fold into a known three-dimensional structure, *Science 253*, 164−170.
35. Luthy, R., Bowie, J. U., and Eisenberg, D. (1992) Assessment of protein models with three-dimensional profiles, *Nature 356*, 83−85.
36. Eisenberg, D., Luthy, R., and Bowie, J. U. (1997) VERIFY3D: assessment of protein models with three-dimensional profiles. A method to identify protein sequences that fold into a known three-dimensional structure, *Methods Enzymol. 277*, 396−404.
37. Thornton, J. M. (1981) Disulphide bridges in globular proteins, *J. Mol. Biol. 151*, 261−287.
38. Murphy, D. M., and Kirley, T. L. (2003) Asparagine 81, an invariant glycosylation site near apyrase conserved region 1, is essential for full enzymatic activity of ecto nucleoside triphosphate diphosphohydrolase 3, *Arch. Biochem. Biophys. 413*, 107−115.
39. Zhong, X., Malhotra, R., Woodruff, R., and Guidotti, G. (2001) Mammalian plasma membrane ecto-nucleoside triphosphate diphosphohydrolase 1, CD39, is not active intracellularly. The N-glycosylation state of CD39 correlates with surface activity and localization, *J. Biol. Chem. 276*, 41518−41525.
40. Wu, J. J., Choi, L. E., and Guidotti, G. (2005) N-linked oligosaccharides affect the enzymatic activity of CD39: diverse interactions between seven N-linked glycosylation sites, *Mol. Biol. Cell 16*, 1661−1672.
41. Maley, F., Trimble, R. B., Tarentino, A. L., and Plummer, T. H., Jr. (1989) Characterization of glycoproteins and their associated oligosaccharides through the use of endoglycosidases, *Anal. Biochem. 180*, 195−204.
42. Helenius, A., and Aebi, M. (2001) Intracellular functions of N-linked glycans, *Science 291*, 2364−2369.
43. Hayes, G. R., Williams, A. M., Lucas, J. J., and Enns, C. A. (1997) Structure of human transferrin receptor oligosaccharides: conservation of site-specific processing, *Biochemistry 36*, 5276−5284.
44. Landon, M. (1977) Cleavage at aspartyl-propyl bonds, in *Methods in Enzymology* (Hirs, C. H. W., and Timasheff, S., Eds.) pp 145−149, Academic Press, New York.
45. Sonderegger, P., Jaussi, R., Gehring, H., Brunschweiler, K., and Christen, P. (1982) Peptide mapping of protein bands from polyacrylamide gel electrophoresis by chemical cleavage in gel pieces and re-electrophoresis, *Anal. Biochem. 122*, 298−301.
46. Pace, C. N. (1990) Conformational stability of globular proteins, *Trends Biochem. Sci. 15*, 14−17.
47. Reddy, P. S., and Corley, R. B. (1998) Assembly, sorting, and exit of oligomeric proteins from the endoplasmic reticulum, *BioEssays 20*, 546−554.
48. Ellgaard, L., Molinari, M., and Helenius, A. (1999) Setting the standards: quality control in the secretory pathway, *Science 286*, 1882−1888.
49. Daiho, T., Yamasaki, K., Saino, T., Kamidochi, M., Satoh, K., Iizuka, H., and Suzuki, H. (2001) Mutations of either or both Cys876 and Cys888 residues of sarcoplasmic reticulum Ca2+-ATPase result in a complete loss of Ca2+ transport activity without a loss of Ca2+-dependent ATPase activity. Role of the CYS876−CYS888 disulfide bond, *J. Biol. Chem. 276*, 32771−32778.
50. Bork, P., Sander, C., and Valencia, A. (1992) An ATPase domain common to prokaryotic cell cycle proteins, sugar kinases, actin, and hsp70 heat shock proteins, *Proc. Natl. Acad. Sci. U.S.A. 89*, 7290−7294.
51. Reizer, J., Reizer, A., Saier, M. H., Jr., Bork, P., and Sander, C. (1993) Exopolyphosphate phosphatase and guanosine pentaphosphate phosphatase belong to the sugar kinase/actin/hsp 70 superfamily, *Trends Biochem. Sci. 18*, 247−248.
52. Handa, M., and Guidotti, G. (1996) Purification and cloning of a soluble ATP-diphosphohydrolase (apyrase) from potato tubers (*Solanum tuberosum*), *Biochem. Biophys. Res. Commun. 218*, 916−923.
53. Schuler, H. (2001) ATPase activity and conformational changes in the regulation of actin, *Biochim. Biophys. Acta*, *1549*, 137−147.
54. Grinthal, A., and Guidotti, G. (2004) Dynamic motions of CD39 transmembrane domains regulate and are regulated by the enzymatic active site, *Biochemistry 43*, 13849−13858.
55. Murphy, D. M., Ivanenkov, V. V., and Kirley, T. L. (2002) Identification of cysteine residues responsible for oxidative cross-linking and chemical inhibition of human nucleoside triphosphate diphosphohydrolase 3, *J. Biol. Chem. 277*, 6162−6169.
56. Kirley, T. L., Yang, F., and Ivanenkov, V. V. (2001) Site-directed mutagenesis of human nucleoside triphosphate diphosphohydrolase 3: the importance of conserved glycine residues and the identification of additional conserved protein motifs in eNTPDases, *Arch. Biochem. Biophys. 395*, 94−102.

BI047487Z